

1 **Biogenic SOA formation through gas-phase oxidation and**  
2 **gas-to-particle partitioning – Comparison between process**  
3 **models of varying complexity**

4  
5 **E. Hermansson<sup>1,2</sup>, P. Roldin<sup>1,3</sup>, A. Rusanen<sup>3</sup>, D. Mogensen<sup>3</sup>, N. Kivekäs<sup>1,\*</sup>, R.**  
6 **Väänänen<sup>3</sup>, M. Boy<sup>3</sup> and E. Swietlicki<sup>1,2</sup>**

7 [1] {Division of Nuclear Physics, Lund University, P.O. Box 118 SE-221 00, Sweden}

8 [2] {Centre for Environmental and Climate Research, Lund University, P.O. Box 118 SE-221 00,  
9 Sweden}

10 [3] {Department of Physics, P.O. Box 64, 00014 University of Helsinki, Finland}

11 [\*] {now at: Atmospheric composition, Finnish Meteorological Institute, P.O. box 503, FI-00101,  
12 Helsinki, Finland}

13 Correspondence to: E. Hermansson (emilie.hermansson@nuclear.lu.se)

14  
15 **Abstract**

16 Biogenic volatile organic compounds (BVOCs) emitted by the vegetation play an important role  
17 for the aerosol mass loadings since the oxidation products of these compounds can take part in  
18 the formation and growth of secondary organic aerosols (SOA). The concentrations and  
19 properties of BVOCs and their oxidation products in the atmosphere are poorly characterized,  
20 which leads to high uncertainties in modeled SOA mass and properties. In this study the  
21 formation of SOA has been modeled along an air mass trajectory over the northern European  
22 boreal forest using two aerosol dynamics box models where the prediction of the condensable  
23 organics from the gas-phase oxidation of BVOC is handled with schemes of varying complexity.  
24 The use of box model simulations along an air mass trajectory allows us to compare, under  
25 atmospheric relevant conditions, different model parameterizations and their effect on SOA

1 formation. The result of the study shows that the modeled mass concentration of SOA is highly  
2 dependent on the organic oxidation scheme used to predict the oxidation products. A near-  
3 explicit treatment of organic gas-phase oxidation (Master Chemical Mechanism version 3.2) was  
4 compared to oxidation schemes that use the volatility basis set (VBS) approach. The resulting  
5 SOA mass modeled with different VBS-schemes varies by a factor of about 7 depending on how  
6 the first generation oxidation products are parameterized and how they subsequently age (e.g.  
7 how fast the gas-phase oxidation products react with the OH-radical, how they respond to  
8 temperature changes and if they are allowed to fragment during the aging process). Since the  
9 VBS approach is frequently used in regional and global climate models due to its relatively  
10 simple treatment of the oxidation products compared to near-explicit oxidation schemes; better  
11 understanding of the abovementioned processes are needed. Based on the result from this study,  
12 fragmentation should be included to get a realistic SOA formation. Furthermore; compared to the  
13 most commonly used VBS-schemes, the near-explicit method produces less - but more oxidized -  
14 SOA.

15

## 16 **1 Introduction**

17 Secondary organic aerosols (SOA), formed through gas-to-particle partitioning in the  
18 atmosphere, constitute a large part of the global organic aerosol load (Crippa et al., 2014;  
19 Hallquist et al., 2009; Jimenez et al., 2009) and affect the climate by absorbing or scattering  
20 radiation and acting as cloud condensation nuclei (CCN) (Scott et al., 2014). Over boreal forests,  
21 with little anthropogenic influences, most particles are comprised of organic constituents  
22 (O'Dowd et al., 2002; Tunved et al., 2006; Yttri et al., 2011), formed when biogenic volatile  
23 organic compounds (BVOCs), such as terpenes, are oxidized to form less volatile compounds.  
24 Despite the importance of SOA as climate forcer, large uncertainties remain about the formation  
25 mechanisms and properties.

26 A lot of effort has been put into gaining better knowledge of how SOA is formed (Hallquist et al.,  
27 2009) and how it can grow nucleation mode particles into CCN (Kerminen et al., 2012). There  
28 are still large uncertainties remaining in the SOA formation process, mostly due to the vast  
29 number of known – but especially unknown – oxidation products of BVOCs. It has therefore  
30 been common practice in global model studies to simplify the gas-phase oxidation using only two

1 hypothetical oxidation products with laboratory constrained equilibrium partitioning coefficients  
2 to estimate the formation of SOA (Kroll and Seinfeld, 2008), based on the two-product model  
3 developed by Odum et al. (1996). This method does not account for continuous oxidation in the  
4 gas or particle-phase and atmospheric models that use this method generally underestimate the  
5 organic aerosol mass (e.g. Heald et al., 2005; Spracklen et al., 2011; Volkamer et al., 2006). To  
6 reduce these limitations, Donahue et al. (2006) proposed a volatility basis set (VBS) approach,  
7 where the oxidation products are sorted into logarithmically spaced volatility bins, making it  
8 possible to represent a wider range of organic compounds in the atmosphere. The gas-phase aging  
9 (i.e.; the continuous gas-phase oxidation of the products) can be taken into consideration by  
10 moving the oxidation products in the volatility space. To account for the reduction in volatility  
11 when functional groups are added during oxidation, these schemes typically move the products  
12 down one volatility bin per oxidation step (Bergström et al., 2012; Lane et al., 2008). Oxidation  
13 might however also lead to fragmentation, and models that only consider functionalization of  
14 biogenic compounds tend to overestimate the SOA mass concentration (Lane et al., 2008;  
15 Murphy and Pandis, 2009). A two-dimensional volatility basis set can be used to keep track of  
16 the oxygen to carbon (O:C) ratio during the aging process (Donahue et al., 2011; Jimenez et al.,  
17 2009), making it possible to also include fragmentation. Studies that have included fragmentation  
18 indicate that it is an important process to consider (Chen et al., 2013; Murphy et al., 2012;  
19 Shrivastava et al., 2013). The abovementioned approaches are however empirical or semi-  
20 empirical and thus rely on experimental studies conducted under environmental conditions that  
21 resemble those in the atmosphere; conditions which might change during the SOA formation  
22 process and during future climate warming.

23 Another way to represent SOA formation is to use a gas-phase mechanism that explicitly predicts  
24 the condensable oxidation products. While this process makes it possible to predict growth under  
25 conditions and timescales beyond those conducted in laboratory studies, it is computationally  
26 heavy and needs to be simplified in order to be applicable (Hallquist et al., 2009). Additionally;  
27 the lack of knowledge of the properties of many oxidation products leads to uncertainties in these  
28 explicit schemes. A number of studies have modeled the SOA formation in chamber experiments  
29 using explicit – or near explicit – gas-phase chemistry (e.g Camredon et al., 2010; Capouet et al.,  
30 2008; Jenkin, 2004; Roldin et al., 2014; Valorso et al., 2011). The discrepancies between the  
31 modeled and measured SOA formation in many of these studies indicate that there exist

1 knowledge gaps that need to be filled in order to better understand the processes behind SOA  
2 formation.

3 In this study uncertain parameters regarding the evolution of the biogenic oxidation products are  
4 identified using two aerosol dynamics box models coupled to different gas-phase oxidation  
5 schemes. The following processes are specifically studied:

- 6 1. The volatility- and oxygenation distribution of stable products formed in the first  
7 oxidation step of  $\alpha$ -pinene oxidation.
- 8 2. The gas-phase aging rate of the abovementioned products with the OH-radical.
- 9 3. The temperature response of the oxidation products.
- 10 4. Fragmentation reactions during the aging process.

11 The aim is to investigate the implementation of different gas-phase oxidation schemes and  
12 condensation schemes of various complexities, and what effect they have on the modeled  
13 evolution of SOA at atmospheric conditions. SOA formation is modeled along an air mass  
14 trajectory over the northern European boreal forest using two aerosol dynamics box models: an  
15 updated version of the Aerosol Dynamics, gas-phase CHEMistry and radiative transfer model  
16 (ADCHEM) (Roldin et al., 2011a) and MALTE-BOX (Boy et al., 2013), which is the zero-  
17 dimensional model version of MALTE (Model to predict new Aerosol formation in the Lower  
18 TropospherE) (Boy et al., 2006). Both models are coupled to the near-explicit Master Chemical  
19 Mechanism version 3.2 (MCMv3.2) (Jenkin et al., 1997; Saunders et al., 2003) which is used  
20 when predicting the oxidation products of the BVOCs (here represented by  $\alpha$ -pinene). Different  
21 VBS approaches, which have all been applied in previous modeling studies, are compared with  
22 near-explicit modeling of SOA formation to get an indication of the uncertainties involved and  
23 the importance of different processes in the VBS regarding SOA formation.

24

## 25 **2 Method**

26 For all simulations in this study, the models were implemented along an air mass trajectory  
27 retrieved from the HYSPLIT-model (Draxler and Rolph, 2013) with meteorological data from the  
28 Global Data Assimilation System (GDAS), downloaded from NOAA Air Resource Laboratory  
29 Real-time Environmental Application and Display sYstem (READY) (Rolph, 2013), linearly  
30 interpolated from 3 hours to 1 min (the main time step used in the simulations).

## 1 **2.1 Model descriptions**

### 2 **2.1.1 ADCHEM**

3 The two-dimensional trajectory model ADCHEM was primarily developed to be used for urban  
4 plume studies in the atmosphere (Roldin et al., 2011b). In order to capture the vertical and  
5 horizontal dispersion of urban plumes, ADCHEM solves the atmospheric diffusion equation  
6 perpendicular to the air-mass trajectory. However, in this study we will only use ADCHEM as a  
7 box model (zero-dimensional). The aerosol dynamics scheme in ADCHEM includes  
8 homogeneous nucleation, dry deposition, Brownian coagulation and detailed  
9 condensation/evaporation. ADCHEM also contains a radiative transfer model which calculates  
10 the spectral actinic flux (for more detailed information about ADCHEM, see Roldin et al.  
11 (2011a)). Different gas-phase oxidation schemes can be coupled to ADCHEM; for more  
12 information about these, and also how the pure-liquid saturation vapor pressures of the  
13 condensing species are estimated, see Sect. 2.3.

14 The condensation/evaporation module in ADCHEM can be combined either with the non-  
15 equilibrium 2DVBS approach, as described in Roldin et al. (2011a), or with a detailed particle-  
16 phase chemistry and kinetic multilayer model (Roldin et al., 2014). The saturation vapor  
17 pressures for each particle size bin are corrected with Raoult's law, taking into account the non-  
18 ideal interactions between compounds in the organic particle phase (activity coefficients) and the  
19 Kelvin effect. In this study we will treat the SOA as a well-mixed liquid, and neglect any  
20 heterogeneous chemistry.

### 21 **2.1.2 MALTE-BOX**

22 MALTE-BOX is a zero-dimensional model based on the one-dimensional column model  
23 MALTE (Boy et al., 2006). The box version is described in Boy et al. (2013) and Wang et al.  
24 (2013). The model consists of modules for gas-phase chemical reactions and photochemistry  
25 together with aerosol dynamics. In this study, emissions of inorganic trace gases and  $\alpha$ -pinene are  
26 treated as explained in Sect. 2.2.1, while the chemistry and the saturation vapor pressures used  
27 are explained in Sect. 2.3.3. The aerosol dynamics in MALTE-BOX is solved by UHMA, which  
28 is described in detail in Korhonen et al. (2004). The model includes Brownian coagulation,

1 condensation/evaporation, dry deposition and several nucleation schemes, however; only  
2 condensation/evaporation was considered in this study. The model uses sectional methods and a  
3 Runge-Kutta solver to solve the general dynamic equation for aerosols.

4 The main difference between UHMA and ADCHEM lies in the various vapor property  
5 parameterizations and additional mechanisms for the activity coefficients in the condensation  
6 algorithm. The densities of the condensing pure organic compounds in UHMA are estimated  
7 based on their molecular weights and atomic volumes, taking into consideration the changes in  
8 volume due to intramolecular bonding (Girolami, 1994). In ADCHEM, on the other hand, the  
9 densities are assumed to be  $1400 \text{ kg/m}^3$  for all condensing organic species (Hallquist et al., 2009).  
10 The models also calculate the molecular diffusion coefficients of the vapors differently;  
11 ADCHEM uses a method described in Jacobson (2005), whereas MALTE-BOX derives them  
12 from Fuller et al. (1966).

## 13 **2.2 Model setup**

14 All model simulations start over the Atlantic Ocean ( $74^{\circ}34' \text{N}$ ,  $10^{\circ}19' \text{W}$ ) the 28 July 2005, 18  
15 UTC. The air mass then passes close to three remote research stations: first Abisko ( $68^{\circ}52' \text{N}$ ,  
16  $18^{\circ}30' \text{E}$ , 360 m above sea level (asl)) on 31 July 2005 at 03 UTC, then Pallas ( $67^{\circ}56' \text{N}$ ,  $24^{\circ}22' \text{E}$ ,  
17 565 m asl) on 31 July 2005 at 18 UTC and finally Värriö ( $67^{\circ}45' \text{N}$ ,  $29^{\circ}38' \text{E}$ , 395 m asl) on 2  
18 August 2005 at 00 UTC, see Fig. 1. The three stations are located on a west-to-east line roughly  
19 200 km apart from each other. Description of the stations and the instrumentation can be found in  
20 Väänänen et al. (2013). Even though the Pallas station is located on a hill top, all three stations  
21 are considered as ground level sites in this study. Since the boundary layer is assumed to be well-  
22 mixed, the air arriving to the stations represents the boundary layer on a larger scale. The specific  
23 trajectory was chosen by analyzing hourly HYSPLIT trajectories (Draxler and Rolph, 2013) from  
24 years 2005-2007 arriving at Värriö at the altitude of the station. The analysis was limited to  
25 trajectories arriving from the Atlantic Ocean and passing over Scandinavia between latitude  
26 parallels  $67^{\circ}6' \text{N}$  and  $69^{\circ} \text{N}$  within 1000 m above ground level in order to ensure similar source  
27 areas and clear transport route between the stations. Furthermore, the trajectories had to pass over  
28 Abisko and Pallas within 25 km from the respective station during its path. This is in line with the  
29 general 10-30% uncertainty of trajectories (Stohl, 1998). The aerosol particle number size  
30 distributions at the three stations were analyzed at the times when the trajectories passed them. A

1 trajectory that had a low particle number concentration in Abisko which increased between the  
2 stations was chosen. Additionally, this trajectory had to remain in the boundary layer between the  
3 stations with no precipitation along its path. The data from Abisko were used as the initial  
4 particle size distribution in the model by using the automatic lognormal fitting algorithm DO-  
5 FIT, version 4.20 (Hussein et al., 2005). Due to the low particle concentration and the origin of  
6 the air mass, it was assumed to have a chemical composition of marine aerosol. O'Dowd et al.  
7 (2004) measured the physical and chemical properties of aerosols at the research station Mace  
8 Head originating from the North Atlantic Ocean during periods of both high and low biological  
9 activity in 2002. The chemical information from their study during periods of high biological  
10 activity (here assumed to represent summer conditions) was used to estimate the particle size  
11 dependent organic fraction. The initial concentrations of the inorganic compounds, not set to  
12 zero, are estimated based on average background concentrations and listed in Table 1.

### 13 **2.2.1 Emissions**

14 The inorganic gas emissions ( $\text{SO}_2$ ,  $\text{NO}_x$  and  $\text{CO}$ ) along the air mass trajectory were retrieved  
15 from the emission database for the year 2005 from EMEP (European Monitoring and Evaluation  
16 Programme). The BVOC emissions, assumed to include only  $\alpha$ -pinene, were estimated using a  
17 method described in Tunved et al. (2006) where the flux of  $\alpha$ -pinene is dependent on the  
18 emission potential of coniferous trees, the biomass density of these species along the trajectory  
19 (estimated to  $950 \text{ g/m}^2$  (Lindfors et al., 1999)) and the ambient temperature. Since the simulations  
20 are done with zero-dimensional models, the  $\alpha$ -pinene emissions were assumed, as in the study by  
21 Tunved et al. (2006), to be confined in a well-mixed boundary layer of a constant height of 1000  
22 meters.

### 23 **2.3 Description of base case simulations**

24 In all simulations MCMv3.2 is used to model the gas phase, i.e.; the inorganic chemistry and the  
25 first oxidation step of  $\alpha$ -pinene. However, the resulting oxidation products from this step, and  
26 their subsequent gas-phase evolution, are modeled with varying complexity. The three schemes  
27 used to model the evolution of these condensable organic oxidation products are listed in Table 2  
28 (1DVBS, 2DVBS and MCM) and used throughout this study as base case simulations. MCM  
29 model the organic oxidation products near-explicitly with MCMv3.2, while the two VBS-

1 approaches, after the first oxidation step of  $\alpha$ -pinene, distribute the products into groups with  
2 different volatility based on chamber measurements. After the products in the VBS simulations  
3 have been distributed in their respective VBS-space due the gas-phase reactions, their  
4 temperature dependent saturation vapor pressures are calculated. These pressures, no longer  
5 bound to the VBS-grid, are used in the condensation/evaporation module. The 2DVBS simulation  
6 is based on the two-dimensional VBS described in Jimenez et al. (2009) and 1DVBS is based on  
7 the one-dimensional VBS scheme used in the EMEP model (Bergström et al., 2012). The  
8 simulations are described in the sections below and, if not otherwise mentioned, coupled to  
9 ADCHEM.

### 10 **2.3.1 1DVBS**

11 The 1DVBS scheme distributes all organic oxidation products between 9 volatility classes  
12 separated by powers of 10 in saturation vapor concentration,  $C^*$ , ranging from  $10^{-5}$  to  $10^3$   $\mu\text{g}/\text{m}^3$ .  
13 The scheme is based on how SOA are treated in the EMEP chemical transport model (Bergström  
14 et al., 2012). The first generation products from the oxidation of  $\alpha$ -pinene and ozone are  
15 distributed according to a 4-product basis set parameterization based on chamber studies (Lane et  
16 al., 2008), see Table 2. The products continue to react with the OH-radical with a reaction rate of  
17  $4 \cdot 10^{-12}$   $\text{cm}^3 \text{molec}^{-1} \text{s}^{-1}$ . At a reference temperature of 298 K, each reaction leads to a  
18 reduction in  $C^*$  by one order of magnitude and a 7.5 % increase in mass due to the added oxygen.  
19 The Clausius Clapeyron equation (see Eq. (A2) in Appendix A) is used to calculate the  
20 temperature dependence with a constant  $\Delta H^{vap}$  of 30 kJ/mol. Fragmentation is not considered.

### 21 **2.3.2 2DVBS**

22 The 2DVBS base case simulation in this study distributes all organic oxidation products across  
23 12 volatility classes separated by powers of 10 in  $C^*$ , ranging from  $10^{-5}$  to  $10^6$   $\mu\text{g}/\text{m}^3$ , and 12  
24 discrete O:C-ratios from 0.1 to 1.2, in steps of 0.1. The first generation products from the  
25 oxidation of  $\alpha$ -pinene by ozone are distributed in the volatility space according to a 7-product  
26 basis set parameterization based on chamber studies (Donahue et al., 2009), see Table 2. In order  
27 to distribute the products in the second dimension (O:C-ratio), Eq. (A1) is used together with the  
28 assumption that most first generation products have the same number of carbon atoms ( $n_C$ ) as the  
29 parent hydrocarbon: here  $\alpha$ -pinene with  $n_C = 10$  (Jimenez et al., 2009). This means that the

1 oxidation of  $\alpha$ -pinene by ozone is assumed to include no fragmentation. Further oxidation in the  
2 gas-phase is based on Jimenez et al. (2009) where the products are assumed to react with the OH-  
3 radical with a reaction rate constant of  $3 \cdot 10^{-11} \text{ cm}^3 \text{ molec}^{-1} \text{ s}^{-1}$ . For more information of  
4 functionalization and fragmentation of the oxidation products, see Appendix A.

### 5 **2.3.3 MCM**

6 The MCM base case simulation considers the degradation of  $\alpha$ -pinene by using the near-explicit  
7 gas-phase kinetic mechanism MCMv3.2, which includes – in the case of  $\alpha$ -pinene degradation -  
8 942 reactions involving 293 organic and 19 inorganic gas-phase compounds. The pure liquid  
9 saturation vapor pressures of the 153 most important oxidation products (the non-radicals that  
10 contribute to particle growth in the condensation scheme) are estimated using a group  
11 contribution method described by Nannoolal et al. (2008). In the first oxidation step,  $\alpha$ -pinene  
12 can react with ozone and the two radicals OH and  $\text{NO}_3$ . The volatility and O:C-ratio distribution  
13 of the first stable, non-radical generation products formed are compared with the first generation  
14 products derived from chamber experiments (which are used in the VBS simulations). In order to  
15 do this, a simulation was done where the first generation products generated in MCMv3.2 did not  
16 continue to react. A low  $\text{NO}_x$  environment was assumed with a constant OH-radical  
17 concentration of  $2 \cdot 10^5 \text{ cm}^{-3}$  (about the average concentration over land in the base case  
18 simulations) and a starting concentration of  $\text{O}_3$  of  $5 \cdot 10^{11} \text{ cm}^{-3}$ . The starting concentration of  $\alpha$ -  
19 pinene was  $8 \cdot 10^9 \text{ cm}^{-3}$ , and the simulation was run for 72 hours to ensure that all  $\alpha$ -pinene had  
20 been consumed. The result of this simulation is discussed in Sect. 3.2.

### 21 **2.4 Processes not investigated in this study**

22 This study explores different ways to model SOA formation through homogeneous gas-phase  
23 reactions and subsequent gas-to-particle partitioning. It is foremost a model comparison study  
24 aimed at investigating the impact that different parameterizations regarding homogeneous gas-  
25 phase reactions have on modeled particle growth. Other processes that may influence the growth  
26 (e.g. emissions, boundary layer meteorology etc.) are treated with relatively simple assumptions.  
27 Moreover; SOA formation of course depends on many other complex processes (e.g. nucleation,  
28 coagulation, dry deposition, particle-phase chemistry etc.), some of them included in this study  
29 but not investigated further. The simulations conducted should therefore not be compared to the

1 measurements presented, but with each other. The measurements are instead shown as an  
2 indicator for realistic particle mass concentrations in boreal environments.

3

### 4 **3 Results and discussion**

5 The influence of the different gas-phase oxidation schemes, described in Sect. 2.3, on the  
6 distribution and properties of the  $\alpha$ -pinene oxidation products is presented in this section. The  
7 subsequent effect on the SOA formation along the chosen air mass trajectory in Fig. 1 is  
8 compared and discussed. Aside from the three base case scenarios listed in Table 2, and described  
9 in Sect. 2.3 above, different sensitivity tests were performed on the 2DVBS to investigate the  
10 impact of different assumptions made in the VBS model setup. Details of these simulations are  
11 listed in Table 3. In all simulations, if not otherwise mentioned, the gas-phase oxidation schemes  
12 were coupled to the aerosol dynamics box model, ADCHEM. First however, the condensation  
13 modules in the two box models ADCHEM and MALTE-BOX will be compared.

#### 14 **3.1 Condensation in ADCHEM and MALTE-BOX**

15 In order to test the sensitivity of the condensation module in ADCHEM, a simulation was done  
16 where the aerosol dynamics box model MALTE-BOX, was coupled to MCMv3.2 instead of  
17 ADCHEM. Condensation was the only aerosol dynamics process included in both box models for  
18 the comparison and the result is shown in Fig. 2. The upper panel shows the volume  
19 concentration of SOA along the trajectory, where the dotted blue line is the result from the  
20 MCM-ADCHEM coupling and the pink, dashed line the result from the MCMv3.2 being coupled  
21 to the MALTE-BOX model. The discrepancy between the modeled mass concentrations is  
22 mainly due to the overall lower densities of condensable organics in MALTE-BOX compared to  
23 those in ADCHEM. These densities are used when the change of particle mass during  
24 condensation (or evaporation) are translated to the corresponding change in particle volume. The  
25 solid blue line in the upper panel in Fig. 2 is the result of using the same method as in MALTE-  
26 BOX to parameterize the densities of the condensing organic oxidation products in ADCHEM  
27 (see Sect. 2.1.2 for more details about the parameterizations). The lower panel in Fig. 2 shows the  
28 number size distribution at different times along the trajectory (represented by different colors).  
29 The smaller particles seem to grow faster in MALTE-BOX compared to those in ADCHEM,

1 especially during nighttime when the temperature is low. Considering the complexities of both  
2 models, they agree fairly well, with a maximum difference in volume concentration of 14 % at t =  
3 129 hours along the trajectory (3rd of August 03 UTC), corresponding to a maximum difference  
4 in the modeled geometric mean diameter of about 10 %.

5 The pure-liquid saturation vapor pressures of each organic oxidation product, needed to model  
6 the condensational growth in near-explicit models, can be estimated using different group  
7 contribution methods, both ADCHEM and MALTE-BOX normally use the method described by  
8 Nannoolal et al. (2008) (see Sect. 2.3.3). In Fig. 3, SOA formation modeled with ADCHEM  
9 using this method is compared to a simulation where ADCHEM instead uses the group  
10 contribution method SIMPOL (Pankow and Asher, 2008). The latter method causes slower SOA  
11 formation since it predicts somewhat higher saturation vapor pressures, illustrating that the  
12 estimation of saturation vapor pressures are uncertain and needs to be investigated further.

13 Moreover; a recent study by Ehn et al. (2014) indicates that the ozonolysis of  $\alpha$ -pinene might lead  
14 to products of extremely low volatility that condense irreversibly to form SOA and thus have the  
15 potential to increase the SOA yield significantly. These products are currently not included in the  
16 model simulations in this study but we are planning to implement them in future studies.

### 17 **3.2 Base case simulations**

18 The growth of SOA along the chosen trajectory, modeled by the three base case scenarios  
19 described in Table 2, is shown in Fig. 4. The figure also includes the calculated mass  
20 concentrations from size distribution measurements in Abisko, Pallas and Värriö at the time the  
21 air mass passed by. The measurements from Pallas and Värriö are further compared with  
22 estimations of particle mass concentrations from two studies: Tunved et al. (2006) and Väänänen  
23 et al. (2013), scaled with the size distribution measurement from Abisko. In both of these studies  
24 the mass concentrations are expressed as a function of time the air mass has spent over land. The  
25 former study bases its expression on measurements conducted during the growing season (April  
26 to September) between 1999 and 2004, and the latter on measurements during the growing season  
27 between 2005 and 2007. Aside from the different measurement periods in the studies, Tunved et  
28 al. (2006) use the same expression to estimate the mass concentration both in Pallas and Värriö,  
29 while Väänänen et al. (2013) generate two separate estimations: one for Pallas and another for

1 Värriö. This resulted in lower estimated mass concentrations in the study by Tunved et al. (2006)  
2 compared to Väänänen et al. (2013), especially in the case of Värriö.

3 Neither the measurements conducted when the air mass passed the site, nor the estimations of the  
4 mass concentration from Tunved et al. (2006) and Väänänen et al. (2013) indicate that the  
5 particle mass concentration should reach the value it does in the 2DVBS simulation. This  
6 simulation also diverges most from the other simulations. In order to understand why the growth  
7 of SOA is higher in the 2DVBS, not only the mass evolution of the particle-phase, but also that of  
8 the gas-phase, needs to be studied.

9 Since a lot of the oxidation products from  $\alpha$ -pinene exist in significant fractions both in the  
10 particle and gas-phase at atmospheric conditions, it is informative to look at how they are  
11 distributed between the two phases depending on the amount of time they have spent over land.  
12 Figures 5b-d show the volatility distribution of the condensable products at the three  
13 measurement sites, modeled by the three base case scenarios. Figure 5a shows the distribution of  
14 the first generation products, i.e.; the first stable, non-radical products from the reaction between  
15  $\alpha$ -pinene and ozone (in MCM, the first oxidation step also includes reaction with the OH-radical  
16 and  $\text{NO}_3$ ). The darker colors in each bar in Figs. 5b-d illustrate the portion of products in the  
17 particle-phase; e.g., in Abisko almost all products are in gas-phase in all three scenarios. As the  
18 air mass moves,  $\alpha$ -pinene is emitted and its oxidation products are accumulated and oxidized;  
19 leading to an increased portion of products partitioning to the particle phase. In Värriö, where the  
20 SOA mass concentration is in the order of magnitude of  $1 \mu\text{g}/\text{m}^3$ , compounds with saturation  
21 concentration lower than  $\sim 10 \mu\text{g}/\text{m}^3$  partition substantially to the particle-phase. The 2DVBS  
22 simulation has about 40% more total mass (gas and particle) in this range in Värriö than the other  
23 two base case simulations. The higher mass is partly due to the different first generation  
24 chemistry between the model scenarios: compared to the other two base case simulations, the first  
25 oxidation step in 2DVBS generates more mass, especially compared to 1DVBS – this will be  
26 discussed further in Sect. 3.3. Most of this “extra” mass is located in high volatility bins and  
27 therefore resides in gas-phase; however, if allowed to age it will increase the particle mass.

28 Here it is also evident that while the evolution of particle mass in the MCM and 1DVBS  
29 simulations in Fig. 4 show similar patterns, the volatility distribution of their oxidation products  
30 does not. The 1DVBS distributes its first generation products more evenly in the volatility space

1 and - due to the relatively simple parameterization of the aging process - the distribution remains  
2 even throughout the simulation. Moreover, the 1DVBS only distributes first generation products  
3 in 4 bins, products with higher volatilities are (in this scheme) assumed to have no effect on the  
4 particle growth and are thus ignored.

5 Gas-phase oxidation does not necessarily lead to products with lower volatility; the more  
6 oxygenated the products are, the higher is the probability that they fragment and form products  
7 with lower carbon number (Kroll et al., 2009). Oxidation does however tend to increase the O:C-  
8 ratio of the products (Kroll et al., 2011; Murphy et al., 2011); thus, the O:C ratio can provide  
9 valuable information on the amount of aging the compounds have experienced. O:C ratio in  
10 regional organic aerosol is about 0.7 (Hallquist et al., 2009).

11 Figure 6 illustrates both the evolution of O:C-ratio and volatility of the oxidation products in the  
12 SOA formation process, where the grey areas represent the state of the first generation oxidation  
13 products (in gas or particle-phase) while the pink ones represent only the particle properties in  
14 Pallas (when the air mass has spent 18 hours over land). The mass-weighted average O:C-ratio of  
15 the first generation products, represented by the stars, are higher in the MCM simulation than in  
16 the 2DVBS. Since the MCM volatility is also higher, this implies that fragmentation could play a  
17 larger role in the MCM in the first oxidation step, which in turn would mean that more oxidation  
18 steps are needed before the products can partition to the particle-phase, causing a higher mass-  
19 weighted average of the O:C-ratio of the resulting products in particle-phase. The first generation  
20 products in the 1DVBS simulation have about the same O:C-ratio as the MCM, however; the  
21 1DVBS does not include fragmentation, instead every oxidation step leads to products with lower  
22 volatilities, but the aging rate is so slow that almost no aging takes place.

23 The time evolution of the mass-weighted average SOA properties along the air mass trajectory  
24 starting from Abisko, modeled by the three base case scenarios, are also shown in Fig. 6. In the  
25 direction of the arrows, the colors indicate how the particle mass concentration changes during  
26 transportation. Except during the first hours, the saturation concentrations in all simulations  
27 slightly increase over time since  $\alpha$ -pinene is continuously emitted along the trajectory. The lower  
28 mole fractions of especially the more volatile organic compounds in the particle phase during the  
29 first hours probably cause the initial decrease in saturation concentrations (Raoult's law). The  
30 MCM and 2DVBS simulations show a stronger diurnal trend in the O:C-ratio due to temperature

1 variations compared to the 1DVBS. This is probably the result of the simpler aging mechanism in  
2 the 1DVBS simulation, e.g.; the use of a constant and low enthalpy of vaporization in the  
3 1DVBS.

### 4 **3.3 2DVBS sensitivity simulations**

5 The results of the sensitivity tests performed on the 2DVBS simulation are presented in this  
6 section. The names and details of these simulations are described in Table 3. The studied  
7 parameters are the first generation chemistry, the aging rate, the enthalpy of vaporization, and the  
8 role of fragmentation in the 2DVBS. The results of these tests are presented in Figs. 7a and 7b.

9 Figure 7a includes results from simulations where different methods have been used to predict  
10 the distribution of first generation products from the oxidation of  $\alpha$ -pinene. The effect of using  
11 the first generation volatility distribution from the 1DVBS base case in the 2DVBS (2DVBS-  
12 1DVBS, green line) is small even though the distributions from the two simulations differ from  
13 each other (see Fig. 5a). This does not mean that the volatility distribution of first generation  
14 products have no influence on how the products evolve in the atmosphere. The distribution from  
15 the 1DVBS causes the first generation oxidation products in the 2DVBS-1DVBS to distribute  
16 toward lower saturation concentrations, which should lead to a higher SOA growth in the  
17 2DVBS-1DVBS than in the base case 2DVBS scenario. However; due to the relationship  
18 between carbon number and volatility in the 2DVBS simulation (Eq. A1) and the assumption that  
19 the oxidation of  $\alpha$ -pinene by ozone do not include fragmentation (i.e.: most first generation  
20 products will have carbon number 9 or 10), the O: C-ratio of the first generation products will be  
21 higher in 2DVBS-1DVBS than in the base case 2DVBS. This is illustrated in Fig. 8 and  
22 explained as follows: Since the carbon number of the products are known, the O:C distribution of  
23 the products can be calculated based on the known volatility distribution of the first generation  
24 products. Figure 8 illustrates how the O:C-ratio is a function of the volatility when the carbon  
25 number is 10 (black line). The first generation products in the 2DVBS-1DVBS (lower panel, Fig.  
26 8) are distributed towards lower volatilities than the 2DVBS (upper panel, Fig. 8) which explain  
27 their higher O:C-ratios. This will cause a larger fraction of products to fragment in higher  
28 generation oxidation reactions compared to the base case scenario (fragmentation ratio =  
29  $O:C^{(1/6)}$ ), leading to a smaller SOA growth in the 2DVBS-1DVBS. The overall difference  
30 between the scenarios is very small.

1 The solid orange line in Fig. 7a shows the resulting growth of SOA when the O:C-ratio of all first  
2 generation products in the 2DVBS simulation are set to 0.4 (2DVBS-OC=0.4). This further  
3 confirms that higher O:C-ratio of first generation products lead to lower SOA mass due to the  
4 increased fragmentation. This initial O:C-ratio is closer to the O:C-ratio of oxidation products  
5 from  $\alpha$ -pinene ozonolysis measured in chamber studies (Chhabra et al., 2010) and also closer to  
6 the corresponding value in the MCM-simulation, implying that fragmentation is important  
7 already in the first oxidation steps.

8 The distribution of the first generation products in the 2DVBS base case scenario, based on  
9 Donahue et al. (2009), are constrained by chamber measurements for the products in the volatility  
10 bins with saturation concentrations ( $C^*$ ) between 1 and 1000  $\mu\text{g}/\text{m}^3$ . Based on mass balance  
11 calculations, Donahue et al. (2009) concludes that the majority of the mass is unaccounted for  
12 and place the remainder of the mass in bins with higher  $C^*$  within the VBS. Products in these bins  
13 are too volatile to partition to the particle-phase; through aging they will however eventually  
14 acquire low enough volatility to condense. The dashed orange line in Fig. 7a (2DVBS-4prod)  
15 implies that the aging of these products is an important process since the particle growth is  
16 reduced when they are excluded. The distribution of the high volatility products are however very  
17 uncertain. Explicit or near-explicit modeling may provide a more realistic method to predict these  
18 products, keeping in mind that these approaches also include uncertainties (such as the estimation  
19 of saturation vapor pressures discussed in Sect. 3.1). In the 2DVBS-MCM simulation, the  
20 distribution of first generation products in the two-dimensional VBS is predicted using  
21 MCMv3.2, while further oxidation is modeled with the 2DVBS. The result of this simulation is  
22 represented by the blue line in Fig. 7a (2DVBS-MCM). The reduction in particle growth is  
23 caused by the, on average, higher  $C^*$  and higher O:C-ratio of the first generation products  
24 modeled by MCMv3.2 compared to the chamber-based mass distribution used in 2DVBS base  
25 case scenario. Overall; the different simulations in Fig. 7a vary with about a factor of three,  
26 highlighting the need for more knowledge of the oxidation products, and their distribution,  
27 already after the first oxidation step.

28 In Fig. 7b, the result of using different aging parameterizations in the VBS is illustrated. The first  
29 generation products are modeled as in the base case 2DVBS. To test how sensitive the 2DVBS  
30 base case scenario is to fragmentation during aging, a simulation without fragmentation (2DVBS-  
31 noFrag; dashed black line) and a simulation when all oxidation steps include fragmentation

1 (2DVBS-maxFrag; black line) were conducted. Without fragmentation, the mass of SOA  
2 increases to unrealistically high values implying that fragmentation is needed in order to predict  
3 realistic values of SOA growth in environments where aging is important for the mass  
4 concentration. The effect of the other extreme (fragmentation occurring in each oxidation step) is  
5 not as big since compounds in the base case scenario with an O:C-ratio of 0.5 (about the average  
6 O:C ratio of SOA in the 2DVBS base case) already have a 89 % fragmentation probability when  
7 oxidized further.

8 Compared to the 2DVBS base case, products in the 1DVBS simulation react with the OH-radical  
9 with one order of magnitude smaller rate constant (based on the aging rate of biogenic SOA in  
10 the EMEP model (Bergström et al., 2012)). Using this one order of magnitude smaller aging rate  
11 (2DVBS-agingRate1DVBS; dashed, green line) causes substantial reduction of SOA mass.  
12 However; since the products do not age much in this scenario the average O:C-ratio of the  
13 resulting particles show even lower values (~0.4) compared to the base case (~0.5). Models that  
14 only distribute SOA mass based on their volatilities (one-dimensional VBS) do not usually  
15 include fragmentation, often forcing them to use unrealistically low aging rates, or exclude aging  
16 of biogenic SOA altogether, to keep SOA concentrations at realistic values (Bergström et al.,  
17 2012; Murphy and Pandis, 2009).

18 In the 2DVBS-temp1DVBS simulation (dotted green line in Fig. 7b) the enthalpy of vaporization  
19 has been set to a constant value of 30 kJ/mole (while keeping everything else as in the 2DVBS  
20 base case). The result is a reduced temperature response of the particle growth, as well as a  
21 somewhat smaller growth; this is due to a distribution of the oxidation products towards higher  
22 volatilities compared to the 2DVBS base scenario which uses a  $\Delta H^{vap}$  that varies with saturation  
23 concentration (65-129 kJ/mole). Donahue et al. (2006) however argue that models which include  
24 many semi-volatile species should use more realistic values of  $\Delta H^{vap}$ , i.e.; values that depend on  
25 the volatility of the products.

26 The assumptions regarding gas-phase aging made in this study have a high impact on the SOA  
27 formation. Further research is needed in order to make more reliable parameterization, especially  
28 when explicit chemistry cannot be used.

29

## 1 4 Conclusions

2 The main conclusions of this study are summarized in Table 4, in which four processes that have  
3 the potential to affect SOA formation are stated: 1) First generation volatility- and oxygenation  
4 distribution of  $\alpha$ -pinene oxidation products, 2) OH reaction rate constant with the gas-phase  
5 oxidation products, 3) Temperature response of the oxidation products and 4) The fraction of  
6 second- and multi-generation reactions that give fragmentation, assuming that fragmentation is  
7 included. The uncertainty and impact these processes have on SOA formation, inferred from the  
8 simulations done, are discussed below and summarized in the table:

- 9 1. In this study first generation oxidation products have been modeled explicitly with  
10 MCMv3.2 and compared to two other studies (Bergström et al., 2012; Donahue et al.,  
11 2009) where the volatility distributions are parameterized using chamber data. Depending  
12 on which method used, the results differed by about a factor of three, implying that the  
13 volatility distribution of the first generation products can have a high impact on SOA  
14 formation. The amount of products created through oxidation of BVOCs makes their  
15 volatility distribution uncertain; especially the experimentally derived distribution of the  
16 products with high volatility ( $C^* > 1000 \mu\text{g}/\text{m}^3$ ) that do not partition to the particle-phase  
17 at atmospheric conditions, but can nevertheless be important for SOA formation if  
18 allowed to oxidize further. The O:C-ratios of the initial oxidation products are also  
19 uncertain parameters. The 2DVBS simulation, based on Jimenez et al. (2009), assumed no  
20 fragmentation during the first oxidation step, while some first oxidation steps in the MCM  
21 included fragmentation. As a result, the mass-weighted average O:C-ratio of the products  
22 were a little bit higher in simulations using MCMv3.2. The higher O:C-ratio resulted in a  
23 slower particle growth when fragmentation in higher generation gas-phase reactions were  
24 included.
- 25 2. The first generation products are further oxidized by reactions in the gas-phase (particle-  
26 phase reactions are not considered in this study). In the VBS-simulations, it was assumed  
27 that the products aged by reacting with the OH-radical with a reaction rate that was  
28 independent of where they were located in the VBS-space. Based on previous studies, two  
29 reaction rate constants were used:  $3 \cdot 10^{-11} \text{ cm}^3 \text{ molec}^{-1} \text{ s}^{-1}$  and  
30  $4 \cdot 10^{-12} \text{ cm}^3 \text{ molec}^{-1} \text{ s}^{-1}$ . The lower rate constant resulted in products with  
31 unrealistically low O:C-ratios and substantially reduced the mass concentration of SOA.

1           When the higher reaction rate constant was applied, the aging effect was comparable to  
2           the aging in the MCM simulation where the products are predicted near-explicitly.

3           3. Temperature will affect the gas-to-particle partitioning. When a VBS-approach is used,  
4           individual product information is lost as they are lumped into bins depending on their  
5           volatility. In the VBS-simulations conducted here, the temperature response was modeled  
6           by either letting all bins respond equally to temperature changes, or respond accordingly  
7           to their saturation concentration. This was controlled by choosing a constant or volatility-  
8           dependent enthalpy of vaporization respectively. In the near-explicit modeling of  
9           oxidation products, the temperature response can be modeled in more detail, where each  
10          specific product can have their own response. When a volatility-dependent temperature  
11          response was used in the VBS, as opposed to letting all products respond equally, the  
12          result was in closer agreement with the result from the near-explicit simulation. The  
13          importance of the temperature response regarding SOA formation depends on the  
14          environment. In a boreal environment, there are many organic semi-volatile compounds,  
15          which makes the compound-dependent temperature response more important.

16          4. The results of this study show that fragmentation is important to include during the aging  
17          process. It has been shown that fragmentation becomes more important the more  
18          oxygenated the compounds are, and a sharp increase in fragmentation going from  
19          products with O:C-ratio of 0 to 0.4 has been observed (Kroll et al., 2009). How to  
20          describe the features of fragmentation, especially in the VBS-approach, is however very  
21          uncertain. Based on the result from this study, fragmentation should be included to get a  
22          realistic SOA formation.

23          Other uncertainties, beyond the scope of this study, include particle-phase chemistry and aerosol  
24          phase state. Studies have shown that these processes have the potential to affect SOA formation  
25          (Chan et al., 2007; Kroll and Seinfeld, 2008; Perraud et al., 2012; Roldin et al., 2014). The  
26          diurnal trend, caused by temperature variation, of the particle mass concentration in the base case  
27          scenarios in this study might in part be a result of excluding particle chemistry and assuming  
28          equilibrium partitioning. If the condensing gas-phase species are allowed to undergo chemical  
29          reactions in the particle phase to form low volatile products, evaporation and re-condensation of  
30          these species will be inhibited.

1 Discrepancies exist between measured and modeled SOA, especially in global model studies,  
 2 indicating a lack of knowledge of certain processes involving SOA formation. All processes  
 3 cannot be included in large, global models, but important processes need to be parameterized and  
 4 included. Box-models with process-based representation of aerosol dynamics and gas- and  
 5 particle-phase chemistry are important tools to find these processes and explore how to best  
 6 parameterize them.

7

## 8 **Appendix A: Functionalization and fragmentation in the 2DVBS-scheme**

9 Each oxidation step, after the oxidation of  $\alpha$ -pinene, in the 2DVBS includes functionalization  
 10 where between 1 and 3 oxygen atoms are added, causing a reduction in saturation vapor  
 11 concentration ( $C^*$ ) and the O:C-ratio to increase. The increase in O:C-ratio depends on the  
 12 number of carbon atoms ( $n_C$ ) in the bin of the reacting compound, which is estimated using a  
 13 simple empirical three-parameter group contribution relationship between the pure compound  
 14 saturation concentration at a reference temperature of 298 K ( $\log_{10} C_{298}^*$ ) and the number of  
 15 carbon and oxygen atoms ( $n_O$ ) (Eq. (A1)) (Donahue et al., 2011):

$$16 \log_{10} C_{298}^* = (n_C^0 - n_C)b_C - n_O b_O \quad (A1)$$

17 where  $n_C^0 = 25$  represents the reference point, defined as the number of carbon atoms in an  
 18 alkane with  $C_{298}^* = 1 \mu\text{g}/\text{m}^3$ .  $b_C = 0.475$  is the slope in the linear relationship between  $\log_{10} C_{298}^*$   
 19 and  $n_C$ , i.e; the effect of increasing the number of carbon atoms by one is a 0.475 decade  
 20 decrease in saturation concentration.  $b_O = 1.7$ ; resulting in a 1.7 decade decrease in saturation  
 21 concentration of each added oxygen. To account for the temperature dependence of the saturation  
 22 concentration, the Clausius Clapeyron equation (Eq. (A2)) is used:

$$23 C^* = C_{298}^* \frac{T_{298}}{T} \exp\left(\frac{\Delta H^{vap}}{R} \left(\frac{1}{T_{298}} - \frac{1}{T}\right)\right) \quad (A2)$$

24 Where  $T_{298}$  is the reference temperature and  $R$  is the ideal gas constant.  $\Delta H^{vap}$  is the enthalpy of  
 25 vaporization assumed to depend on  $C_{298}^*$  (Donahue et al., 2006) (see Table 2).

26 After the functionalization step, a fraction ( $f$ ) of the products formed can fragment into at least  
 27 two products with lower carbon number. This fraction is an uncertain parameter, but, as  
 28 suggested by Jimenez et al. (2009), treated as a function of the O:C-ratio of the products:  $f =$

1 O:C<sup>(1/6)</sup>. Figure A1 illustrates the fragmentation probability as a function of the O:C-ratio, where  
2 the range of O:C-ratios of first generation products in the 2DVBS is represented by the shaded  
3 area. As described in Jimenez et al. (2009), the C-C cleavage is assumed to have equal  
4 probability to take place anywhere along the carbon backbone and the resulting products will  
5 have higher volatility than the reactant. Unlike in Jimenez et al. (2009), we however assume that  
6 the fragmentation does not change the O:C-ratio of the products.

## 7 **Acknowledgements**

8 This work was carried out with the support by Nordic Center of Excellence program (CRAICC –  
9 Cryosphere-Atmosphere Interactions in a Changing Arctic Climate), the EU FP7 projects  
10 ACTRIS (Aerosols, Clouds, and Trace gases Research Infra Structure Network) and the  
11 European Commission Seventh Framework Programme (FP7) in the project PEGASOS (Pan-  
12 European gas-aerosols-climate interaction study), the Swedish Strategic Research Program  
13 MERGE, Modeling the Regional and Global Earth System, and the Lund Centre for studies of  
14 Carbon Cycle and Climate Interaction – LUCCI. We also gratefully acknowledge the support by  
15 the Swedish Research Council and the Helsinki University Centre for Environment (HENVI),  
16 Academy of Finland Centre of Excellence program (project No. 1118615).

17 The authors would like to thank Almut Arneth at Karlsruhe Institute of Technology for the size  
18 distribution measurements at Abisko, Heikki Lihavainen at the Finnish Meteorological Institute  
19 for the measurement at Pallas and Markku Kulmala and Pasi Aalto at University of Helsinki for  
20 the measurement at Värriö.

21

## 1 References

- 2 Bergström, R., Denier van der Gon, H. A. C., Prévôt, A. S. H., Yttri, K. E. and Simpson, D.:  
3 Modelling of organic aerosols over Europe (2002–2007) using a volatility basis set (VBS)  
4 framework: application of different assumptions regarding the formation of secondary organic  
5 aerosol, *Atmos. Chem. Phys.*, 12(18), 8499–8527, doi:10.5194/acp-12-8499-2012, 2012.
- 6 Boy, M., Hellmuth, O., Korhonen, H., Nilsson, E. D., ReVelle, D., Turnipseed, A., Arnold, F.  
7 and Kulmala, M.: MALTE – model to predict new aerosol formation in the lower troposphere,  
8 *Atmos. Chem. Phys.*, 6(12), 4499–4517, doi:10.5194/acp-6-4499-2006, 2006.
- 9 Boy, M., Mogensen, D., Smolander, S., Zhou, L., Nieminen, T., Paasonen, P., Plass-Dülmer, C.,  
10 Sipilä, M., Petäjä, T., Mauldin, L., Berresheim, H. and Kulmala, M.: Oxidation of SO<sub>2</sub> by  
11 stabilized Criegee intermediate (sCI) radicals as a crucial source for atmospheric sulfuric acid  
12 concentrations, *Atmos. Chem. Phys.*, 13(7), 3865–3879, doi:10.5194/acp-13-3865-2013, 2013.
- 13 Camredon, M., Hamilton, J. F., Alam, M. S., Wyche, K. P., Carr, T., White, I. R., Monks, P. S.,  
14 Rickard, A. R. and Bloss, W. J.: Distribution of gaseous and particulate organic composition  
15 during dark  $\alpha$ -pinene ozonolysis, *Atmos. Chem. Phys.*, 10(6), 2893–2917, doi:10.5194/acp-10-  
16 2893-2010, 2010.
- 17 Capouet, M., Müller, J.-F., Ceulemans, K., Compernelle, S., Vereecken, L. and Peeters, J.:  
18 Modeling aerosol formation in alpha-pinene photo-oxidation experiments, *J. Geophys. Res.*,  
19 113(D2), D02308, doi:10.1029/2007JD008995, 2008.
- 20 Chan, A. W. H., Kroll, J. H., Ng, N. L. and Seinfeld, J. H.: Kinetic modeling of secondary  
21 organic aerosol formation: effects of particle- and gas-phase reactions of semivolatile products,  
22 *Atmos. Chem. Phys.*, 7(15), 4135–4147, doi:10.5194/acp-7-4135-2007, 2007.
- 23 Chen, S., Brune, W. H., Lambe, A. T., Davidovits, P. and Onasch, T. B.: Modeling organic  
24 aerosol from the oxidation of  $\alpha$ -pinene in a Potential Aerosol Mass (PAM) chamber, *Atmos.*  
25 *Chem. Phys.*, 13(9), 5017–5031, doi:10.5194/acp-13-5017-2013, 2013.
- 26 Chhabra, P. S., Flagan, R. C. and Seinfeld, J. H.: Elemental analysis of chamber organic aerosol  
27 using an aerodyne high-resolution aerosol mass spectrometer, *Atmos. Chem. Phys.*, 10(9), 4111–  
28 4131, doi:10.5194/acp-10-4111-2010, 2010.
- 29 Crippa, M., Canonaco, F., Lanz, V. A., Äijälä, M., Allan, J. D., Carbone, S., Capes, G., Ceburnis,  
30 D., Dall’Osto, M., Day, D. A., DeCarlo, P. F., Ehn, M., Eriksson, A., Freney, E., Hildebrandt  
31 Ruiz, L., Hillamo, R., Jimenez, J. L., Junninen, H., Kiendler-Scharr, A., Kortelainen, A.-M.,  
32 Kulmala, M., Laaksonen, A., Mensah, A. A., Mohr, C., Nemitz, E., O’Dowd, C., Ovadnevaite, J.,  
33 Pandis, S. N., Petäjä, T., Poulain, L., Saarikoski, S., Sellegri, K., Swietlicki, E., Tiitta, P.,  
34 Worsnop, D. R., Baltensperger, U. and Prévôt, A. S. H.: Organic aerosol components derived  
35 from 25 AMS data sets across Europe using a consistent ME-2 based source apportionment  
36 approach, *Atmos. Chem. Phys.*, 14(12), 6159–6176, doi:10.5194/acp-14-6159-2014, 2014.

- 1 Donahue, N. M., Epstein, S. A., Pandis, S. N. and Robinson, A. L.: A two-dimensional volatility  
2 basis set: 1. organic-aerosol mixing thermodynamics, *Atmos. Chem. Phys.*, 11(7), 3303–3318,  
3 doi:10.5194/acp-11-3303-2011, 2011.
- 4 Donahue, N. M., Robinson, A. L. and Pandis, S. N.: Atmospheric organic particulate matter:  
5 From smoke to secondary organic aerosol, *Atmos. Environ.*, 43(1), 94–106,  
6 doi:10.1016/j.atmosenv.2008.09.055, 2009.
- 7 Donahue, N. M., Robinson, A. L., Stanier, C. O. and Pandis, S. N.: Coupled Partitioning,  
8 Dilution, and Chemical Aging of Semivolatile Organics, *Environ. Sci. Technol.*, 40(8), 2635–  
9 2643, doi:10.1021/es052297c, 2006.
- 10 Draxler, R. . and Rolph, G. D.: HYSPLIT (HYbrid Single-Particle Lagrangian Integrated  
11 Trajectory) Model access via NOAA ARL READY Website, NOAA Air Resour. Lab. Silver  
12 Spring, MD [online] Available from: <http://ready.arl.noaa.gov/HYSPLIT.php>, 2013.
- 13 Ehn, M., Thornton, J. A., Kleist, E., Sipilä, M., Junninen, H., Pullinen, I., Springer, M., Rubach,  
14 F., Tillmann, R., Lee, B., Lopez-Hilfiker, F., Andres, S., Acir, I.-H., Rissanen, M., Jokinen, T.,  
15 Schobesberger, S., Kangasluoma, J., Kontkanen, J., Nieminen, T., Kurtén, T., Nielsen, L. B.,  
16 Jørgensen, S., Kjaergaard, H. G., Canagaratna, M., Maso, M. D., Berndt, T., Petäjä, T., Wahner,  
17 A., Kerminen, V.-M., Kulmala, M., Worsnop, D. R., Wildt, J. and Mentel, T. F.: A large source  
18 of low-volatility secondary organic aerosol., *Nature*, 506(7489), 476–479,  
19 doi:10.1038/nature13032, 2014.
- 20 Fuller, E. N., Schettler, P. D. and Giddings, J. C.: NEW METHOD FOR PREDICTION OF  
21 BINARY GAS-PHASE DIFFUSION COEFFICIENTS, *Ind. Eng. Chem.*, 58(5), 18–27,  
22 doi:10.1021/ie50677a007, 1966.
- 23 Girolami, G. S.: A Simple “Back of the Envelope” Method for Estimating the Densities and  
24 Molecular Volumes of Liquids and Solids, *J. Chem. Educ.*, 71(11), 962–964,  
25 doi:10.1021/ed071p962, 1994.
- 26 Hallquist, M., Wenger, J. C., Baltensperger, U., Rudich, Y., Simpson, D., Claeys, M., Dommen,  
27 J., Donahue, N. M., George, C., Goldstein, A. H., Hamilton, J. F., Herrmann, H., Hoffmann, T.,  
28 Iinuma, Y., Jang, M., Jenkin, M. E., Jimenez, J. L., Kiendler-Scharr, A., Maenhaut, W.,  
29 McFiggans, G., Mentel, T. F., Monod, A., Prévôt, A. S. H., Seinfeld, J. H., Surratt, J. D.,  
30 Szmigielski, R. and Wildt, J.: The formation, properties and impact of secondary organic aerosol:  
31 current and emerging issues, *Atmos. Chem. Phys.*, 9(14), 5155–5236, doi:10.5194/acp-9-5155-  
32 2009, 2009.
- 33 Heald, C. L., Jacob, D. J., Park, R. J., Russell, L. M., Huebert, B. J., Seinfeld, J. H., Liao, H. and  
34 Weber, R. J.: A large organic aerosol source in the free troposphere missing from current models,  
35 *Geophys. Res. Lett.*, 32(18), L18809, doi:10.1029/2005GL023831, 2005.

- 1 Hussein, T., Maso, M. D., Petäjä, T., Koponen, I. K., Paatero, P., Aalto, P. P., Hämeri, K. and  
2 Kulmala, M.: Evaluation of an automatic algorithm for fitting the particle number size  
3 distributions, *Boreal environ.*, 10(October), 337–355, 2005.
- 4 Jacobson, M. Z.: *Fundamentals of atmospheric modeling*, Second edi., Cambridge University  
5 Press, New York., 2005.
- 6 Jenkin, M. E.: Modelling the formation and composition of secondary organic aerosol from  $\alpha$ -  
7 and  $\beta$ -pinene ozonolysis using MCM v3, *Atmos. Chem. Phys.*, 4(7), 1741–1757,  
8 doi:10.5194/acp-4-1741-2004, 2004.
- 9 Jenkin, M. E., Saunders, S. M. and Pilling, M. J.: The tropospheric degradation of volatile  
10 organic compounds: a protocol for mechanism development, *Atmos. Environ.*, 31(1), 81–104,  
11 doi:10.1016/S1352-2310(96)00105-7, 1997.
- 12 Jimenez, J. L., Canagaratna, M. R., Donahue, N. M., Prevot, A. S. H., Zhang, Q., Kroll, J. H.,  
13 DeCarlo, P. F., Allan, J. D., Coe, H., Ng, N. L., Aiken, A. C., Docherty, K. S., Ulbrich, I. M.,  
14 Grieshop, A. P., Robinson, A. L., Duplissy, J., Smith, J. D., Wilson, K. R., Lanz, V. A., Hueglin,  
15 C., Sun, Y. L., Tian, J., Laaksonen, A., Raatikainen, T., Rautiainen, J., Vaattovaara, P., Ehn, M.,  
16 Kulmala, M., Tomlinson, J. M., Collins, D. R., Cubison, M. J., Dunlea, E. J., Huffman, J. A.,  
17 Onasch, T. B., Alfarra, M. R., Williams, P. I., Bower, K., Kondo, Y., Schneider, J., Drewnick, F.,  
18 Borrmann, S., Weimer, S., Demerjian, K., Salcedo, D., Cottrell, L., Griffin, R., Takami, A.,  
19 Miyoshi, T., Hatakeyama, S., Shimono, A., Sun, J. Y., Zhang, Y. M., Dzepina, K., Kimmel, J. R.,  
20 Sueper, D., Jayne, J. T., Herndon, S. C., Trimborn, A. M., Williams, L. R., Wood, E. C.,  
21 Middlebrook, A. M., Kolb, C. E., Baltensperger, U. and Worsnop, D. R.: Evolution of organic  
22 aerosols in the atmosphere., *Science*, 326(5959), 1525–1529, doi:10.1126/science.1180353, 2009.
- 23 Kerminen, V.-M., Paramonov, M., Anttila, T., Riipinen, I., Fountoukis, C., Korhonen, H., Asmi,  
24 E., Laakso, L., Lihavainen, H., Swietlicki, E., Svenningsson, B., Asmi, A., Pandis, S. N.,  
25 Kulmala, M. and Petäjä, T.: Cloud condensation nuclei production associated with atmospheric  
26 nucleation: a synthesis based on existing literature and new results, *Atmos. Chem. Phys.*, 12(24),  
27 12037–12059, doi:10.5194/acp-12-12037-2012, 2012.
- 28 Korhonen, H., Lehtinen, K. E. J. and Kulmala, M.: Multicomponent aerosol dynamics model  
29 UHMA: model development and validation, *Atmos. Chem. Phys.*, 4(3), 757–771,  
30 doi:10.5194/acp-4-757-2004, 2004.
- 31 Kroll, J. H., Donahue, N. M., Jimenez, J. L., Kessler, S. H., Canagaratna, M. R., Wilson, K. R.,  
32 Altieri, K. E., Mazzoleni, L. R., Wozniak, A. S., Bluhm, H., Mysak, E. R., Smith, J. D., Kolb, C.  
33 E. and Worsnop, D. R.: Carbon oxidation state as a metric for describing the chemistry of  
34 atmospheric organic aerosol., *Nat. Chem.*, 3(2), 133–139, doi:10.1038/nchem.948, 2011.
- 35 Kroll, J. H. and Seinfeld, J. H.: Chemistry of secondary organic aerosol: Formation and evolution  
36 of low-volatility organics in the atmosphere, *Atmos. Environ.*, 42(16), 3593–3624,  
37 doi:10.1016/j.atmosenv.2008.01.003, 2008.

- 1 Kroll, J. H., Smith, J. D., Che, D. L., Kessler, S. H., Worsnop, D. R. and Wilson, K. R.:  
2 Measurement of fragmentation and functionalization pathways in the heterogeneous oxidation of  
3 oxidized organic aerosol., *Phys. Chem. Chem. Phys.*, 11(36), 8005–8014, doi:10.1039/b905289e,  
4 2009.
- 5 Lane, T. E., Donahue, N. M. and Pandis, S. N.: Simulating secondary organic aerosol formation  
6 using the volatility basis-set approach in a chemical transport model, *Atmos. Environ.*, 42(32),  
7 7439–7451, doi:10.1016/j.atmosenv.2008.06.026, 2008.
- 8 Lindfors, V., Rinne, J. and Laurila, T.: Upscaling the BIPHOREP Results—Regional Biogenic  
9 VOC Emissions in the European Boreal Zone, *Eur. Comm.*, Brussels, 127–150, 1999.
- 10 Murphy, B. N., Donahue, N. M., Fountoukis, C., Dall’Osto, M., O’Dowd, C., Kiendler-Scharr, A.  
11 and Pandis, S. N.: Functionalization and fragmentation during ambient organic aerosol aging:  
12 application of the 2-D volatility basis set to field studies, *Atmos. Chem. Phys.*, 12(22), 10797–  
13 10816, doi:10.5194/acp-12-10797-2012, 2012.
- 14 Murphy, B. N., Donahue, N. M., Fountoukis, C. and Pandis, S. N.: Simulating the oxygen content  
15 of ambient organic aerosol with the 2D volatility basis set, *Atmos. Chem. Phys.*, 11(15), 7859–  
16 7873, doi:10.5194/acp-11-7859-2011, 2011.
- 17 Murphy, B. N. and Pandis, S. N.: Simulating the Formation of Semivolatile Primary and  
18 Secondary Organic Aerosol in a Regional Chemical Transport Model, *Environ. Sci. Technol.*,  
19 43(13), 4722–4728, doi:10.1021/es803168a, 2009.
- 20 Nannoolal, Y., Rarey, J. and Ramjugernath, D.: Estimation of pure component properties, *Fluid  
21 Phase Equilib.*, 269(1-2), 117–133, doi:10.1016/j.fluid.2008.04.020, 2008.
- 22 O’Dowd, C. D., Aalto, P., Hmeri, K., Kulmala, M. and Hoffmann, T.: Aerosol formation:  
23 atmospheric particles from organic vapours., *Nature*, 416(6880), 497–498, doi:10.1038/416497a,  
24 2002.
- 25 O’Dowd, C. D., Facchini, M. C., Cavalli, F., Ceburnis, D., Mircea, M., Decesari, S., Fuzzi, S.,  
26 Yoon, Y. J. and Putaud, J.-P.: Biogenically driven organic contribution to marine aerosol.,  
27 *Nature*, 431(7009), 676–680, doi:10.1038/nature02959, 2004.
- 28 Odum, J. R., Hoffmann, T., Bowman, F., Collins, D., Flagan, R. C. and Seinfeld, J. H.:  
29 Gas/Particle Partitioning and Secondary Organic Aerosol Yields, *Environ. Sci. Technol.*, 30(8),  
30 2580–2585, doi:10.1021/es950943+, 1996.
- 31 Pankow, J. F. and Asher, W. E.: SIMPOL.1: a simple group contribution method for predicting  
32 vapor pressures and enthalpies of vaporization of multifunctional organic compounds, *Atmos.  
33 Chem. Phys.*, 8(10), 2773–2796, doi:10.5194/acp-8-2773-2008, 2008.
- 34 Perraud, V., Bruns, E. a., Ezell, M. J., Johnson, S. N., Yu, Y., Alexander, M. L., Zelenyuk, A.,  
35 Imre, D., Chang, W. L., Dabdub, D., Pankow, J. F. and Finlayson-Pitts, B. J.: Nonequilibrium

- 1 atmospheric secondary organic aerosol formation and growth., Proc. Natl. Acad. Sci. U. S. A.,  
2 109(8), 2836–41, 2012.
- 3 Roldin, P., Eriksson, A. C., Nordin, E. Z., Hermansson, E., Mogensen, D., Rusanen, A., Boy, M.,  
4 Swietlicki, E., Svenningsson, B., Zelenyuk, A. and Pagels, J.: Modelling non-equilibrium  
5 secondary organic aerosol formation and evaporation with the aerosol dynamics, gas- and  
6 particle-phase chemistry kinetic multilayer model ADCHAM, Atmos. Chem. Phys., 14(15),  
7 7953–7993, doi:10.5194/acp-14-7953-2014, 2014.
- 8 Roldin, P., Swietlicki, E., Schurgers, G., Arneth, A., Lehtinen, K. E. J., Boy, M. and Kulmala,  
9 M.: Development and evaluation of the aerosol dynamics and gas phase chemistry model  
10 ADCHEM, Atmos. Chem. Phys., 11(12), 5867–5896, doi:10.5194/acp-11-5867-2011, 2011a.
- 11 Roldin, P., Swietlicki, E., Massling, A., Kristensson, A., Löndahl, J., Eriksson, A., Pagels, J. and  
12 Gustafsson, S.: Aerosol ageing in an urban plume – implication for climate, Atmos. Chem. Phys.,  
13 11(12), 5897–5915, doi:10.5194/acp-11-5897-2011, 2011b.
- 14 Rolph, G. D.: NOAA Air Resource Laboratory Real-time Environmental Application and  
15 Display sYstem (READY) Website (<http://www.ready.noaa.gov>), NOAA Air Resources  
16 Laboratory, Collage Park, MD., 2013.
- 17 Saunders, S. M., Jenkin, M. E., Derwent, R. G. and Pilling, M. J.: Protocol for the development  
18 of the Master Chemical Mechanism, MCM v3 (Part A): tropospheric degradation of non-aromatic  
19 volatile organic compounds, Atmos. Chem. Phys., 3(1), 161–180, doi:10.5194/acp-3-161-2003,  
20 2003.
- 21 Scott, C. E., Rap, A., Spracklen, D. V., Forster, P. M., Carslaw, K. S., Mann, G. W., Pringle, K.  
22 J., Kivekäs, N., Kulmala, M., Lihavainen, H. and Tunved, P.: The direct and indirect radiative  
23 effects of biogenic secondary organic aerosol, Atmos. Chem. Phys., 14(1), 447–470,  
24 doi:10.5194/acp-14-447-2014, 2014.
- 25 Shrivastava, M., Zelenyuk, A., Imre, D., Easter, R., Beranek, J., Zaveri, R. A. and Fast, J.:  
26 Implications of low volatility SOA and gas-phase fragmentation reactions on SOA loadings and  
27 their spatial and temporal evolution in the atmosphere, J. Geophys. Res. Atmos., 118(8), 3328–  
28 3342, doi:10.1002/jgrd.50160, 2013.
- 29 Simpson, D., Benedictow, A., Berge, H., Bergström, R., Emberson, L. D., Fagerli, H., Flechard,  
30 C. R., Hayman, G. D., Gauss, M., Jonson, J. E., Jenkin, M. E., Nyíri, A., Richter, C., Semeena, V.  
31 S., Tsyro, S., Tuovinen, J.-P., Valdebenito, Á. and Wind, P.: The EMEP MSC-W chemical  
32 transport model – technical description, Atmos. Chem. Phys., 12(16), 7825–7865,  
33 doi:10.5194/acp-12-7825-2012, 2012.
- 34 Spracklen, D. V., Jimenez, J. L., Carslaw, K. S., Worsnop, D. R., Evans, M. J., Mann, G. W.,  
35 Zhang, Q., Canagaratna, M. R., Allan, J., Coe, H., McFiggans, G., Rap, A. and Forster, P.:  
36 Aerosol mass spectrometer constraint on the global secondary organic aerosol budget, Atmos.  
37 Chem. Phys., 11(23), 12109–12136, doi:10.5194/acp-11-12109-2011, 2011.

- 1 Stohl, A.: Computation, accuracy and applications of trajectories—A review and bibliography,  
2 Atmos. Environ., 32(6), 947–966, 1998.
- 3 Tunved, P., Hansson, H.-C., Kerminen, V.-M., Ström, J., Maso, M. D., Lihavainen, H., Viisanen,  
4 Y., Aalto, P. P., Komppula, M. and Kulmala, M.: High natural aerosol loading over boreal  
5 forests., Science, 312(5771), 261–263, doi:10.1126/science.1123052, 2006.
- 6 Valorso, R., Aumont, B., Camredon, M., Raventos-Duran, T., Mouchel-Vallon, C., Ng, N. L.,  
7 Seinfeld, J. H., Lee-Taylor, J. and Madronich, S.: Explicit modelling of SOA formation from  $\alpha$ -  
8 pinene photooxidation: sensitivity to vapour pressure estimation, Atmos. Chem. Phys., 11(14),  
9 6895–6910, doi:10.5194/acp-11-6895-2011, 2011.
- 10 Volkamer, R., Jimenez, J. L., San Martini, F., Dzepina, K., Zhang, Q., Salcedo, D., Molina, L. T.,  
11 Worsnop, D. R. and Molina, M. J.: Secondary organic aerosol formation from anthropogenic air  
12 pollution: Rapid and higher than expected, Geophys. Res. Lett., 33(17), L17811,  
13 doi:10.1029/2006GL026899, 2006.
- 14 Väänänen, R., Kyrö, E.-M., Nieminen, T., Kivekäs, N., Junninen, H., Virkkula, A., Dal Maso,  
15 M., Lihavainen, H., Viisanen, Y., Svenningsson, B., Holst, T., Arneth, A., Aalto, P. P., Kulmala,  
16 M. and Kerminen, V.-M.: Analysis of particle size distribution changes between three  
17 measurement sites in northern Scandinavia, Atmos. Chem. Phys., 13(23), 11887–11903,  
18 doi:10.5194/acp-13-11887-2013, 2013.
- 19 Wang, Z. B., Hu, M., Mogensen, D., Yue, D. L., Zheng, J., Zhang, R. Y., Liu, Y., Yuan, B., Li,  
20 X., Shao, M., Zhou, L., Wu, Z. J., Wiedensohler, A. and Boy, M.: The simulations of sulfuric  
21 acid concentration and new particle formation in an urban atmosphere in China, Atmos. Chem.  
22 Phys., 13(21), 11157–11167, doi:10.5194/acp-13-11157-2013, 2013.
- 23 Yttri, K. E., Simpson, D., Nøjgaard, J. K., Kristensen, K., Genberg, J., Stenström, K., Swietlicki,  
24 E., Hillamo, R., Aurela, M., Bauer, H., Offenberg, J. H., Jaoui, M., Dye, C., Eckhardt, S.,  
25 Burkhardt, J. F., Stohl, A. and Glasius, M.: Source apportionment of the summer time  
26 carbonaceous aerosol at Nordic rural background sites, Atmos. Chem. Phys., 11(24), 13339–  
27 13357, doi:10.5194/acp-11-13339-2011, 2011.

28

29

1 Table 1. Initial concentrations applied to all model simulations.

Inorganic species	NO	NO <sub>2</sub>	SO <sub>2</sub>	CO	O <sub>3</sub>	H <sub>2</sub> O <sub>2</sub>	HNO <sub>3</sub>
Concentration [ppb]	0.1	0.2	0.2	100	20	0.1	0.1

2

3

1 Table 2. Details of the three base case gas-phase schemes investigated in this study

Scenarios	Organic oxidation products	1:st generation chemistry	Higher order generation chemistry (aging)
1DVBS (Simpson et al., 2012)	9 products distributed in a 1DVBS, with temperature dependence explained by: $\Delta H_{Eff}^{vap} = 30$ kJ/mol (Bergström et al., 2012)	4-product basis set: $\alpha_{mass} = [0.072 \ 0.061 \ 0.239 \ 0.405]$ for $\log_{10} C_{298}^*$ 0 to 3 (Lane et al., 2008)	Aging rate: $k_{OH} = 4 \cdot 10^{-12} \text{cm}^3 \text{molec}^{-1} \text{s}^{-1}$ (Bergström et al., 2012)
2DVBS (Jimenez et al., 2009)	144 products distributed in a 2DVBS, with temperature dependence explained by: $\Delta H^{vap} = -5.8 \log_{10} C_0^* + 100$ kJ/mol (Donahue et al., 2006)	7-product basis set: $\alpha_{mass} = [0.05 \ 0.085 \ 0.125 \ 0.19 \ 0.4 \ 0.35 \ 0.2]$ for $\log_{10} C_{298}^*$ 0 to 6 (Donahue et al., 2009)	Aging rate: $k_{OH} = 3 \cdot 10^{-11} \text{cm}^3 \text{molec}^{-1} \text{s}^{-1}$ (Jimenez et al., 2009)
MCM (Jenkin et al., 1997; Saunders et al., 2003)	153 products with vapor pressures estimated from Nannoolal et al. (2008)	MCMv3.2	MCMv3.2

2

3

1 Table 3. Sensitivity test performed on the 2DVBS base case (top row). Changed parameters are  
 2 described in bold text, all other parameters are kept unchanged.

Scenario	Organic oxidation products	First generation chemistry	Higher order generation chemistry (aging)
2DVBS	144 products in a 2DVBS, with temperature dependence: $\Delta H^{vap} = -5.8 \log_{10} C_{298}^* + 100$ kJ/mol (Donahue et al., 2006)	7-product basis set: $\alpha_{mass} = [0.05 \ 0.085 \ 0.125 \ 0.19 \ 0.4 \ 0.35 \ 0.2]$ for $\log_{10} C_{298}^*$ 0 to 6 (Donahue et al., 2009) $O:C = f(\log_{10} C_{298}^*)^1$	Aging rate: $k_{OH} = 3 \cdot 10^{-11} \text{cm}^3 \text{molec}^{-1} \text{s}^{-1}$ (Jimenez et al., 2009) Fragmentation ratio = $O:C^{(1/6)}$
2DVBS-OC=0.4	See 2DVBS	<b>O:C = 0.4</b> (Chhabra et al., 2010)	See 2DVBS
2DVBS-4prod	See 2DVBS	<b>4-product basis set:</b> $\alpha_{mass} = [0.05 \ 0.085 \ 0.125 \ 0.19]$ (Donahue et al., 2009) but not including products in bins with $C^* > 10^3$	See 2DVBS
2DVBS-1DVBS	See 2DVBS	<b>4-product basis set:</b> $\alpha_{mass} = [0.072 \ 0.061 \ 0.239 \ 0.405]$ for $\log_{10} C_{298}^*$ 0 to 3 (Lane et al., 2008)	See 2DVBS
2DVBS-MCM	See 2DVBS	<b>First generation product distribution from MCMv3.2:</b> $\alpha_{mole} = [0.0036 \ 0.062 \ 0.0343 \ 0.0266 \ 0.0975 \ 0.294 \ 0.204 \ 0.368]$ for $\log_{10} C_{298}^*$ -1 to 6	See 2DVBS
2DVBS-maxFrag	See 2DVBS	See 2DVBS	<b>Fragmentation ratio = 1</b>
2DVBS-noFrag	See 2DVBS	See 2DVBS	<b>Fragmentation ratio = 0</b>
2DVBS-agingRate1DVBS	See 2DVBS	See 2DVBS	<b>Aging rate: <math>k_{OH} = 4 \cdot 10^{-12} \text{cm}^3 \text{molec}^{-1} \text{s}^{-1}</math></b> (Bergström et al., 2012)
2DVBS-temp1DVBS	<b>144 products in a 2DVBS, with temperature dependence:</b> $\Delta H_{Eff}^{vap} = 30$ kJ/mol (Bergström et al., 2012)	See 2DVBS	See 2DVBS

3 <sup>1</sup>Derived from Eq. (A1), using the volatility distribution from the 7-product basis set together with the assumption  
 4 that most first oxidation steps do not include fragmentation, i.e.; each first generation product ends up in the O:C-bin  
 5 closest to having 10 carbon atoms at its specific saturation concentration.  
 6

1 Table 4. Importance of processes that affect particle mass concentration when modeling long-  
 2 term aging of biogenic SOA in the atmosphere. The uncertainties of the processes are mostly  
 3 based on results from this study, where processes placed to the left are the most uncertain.

---

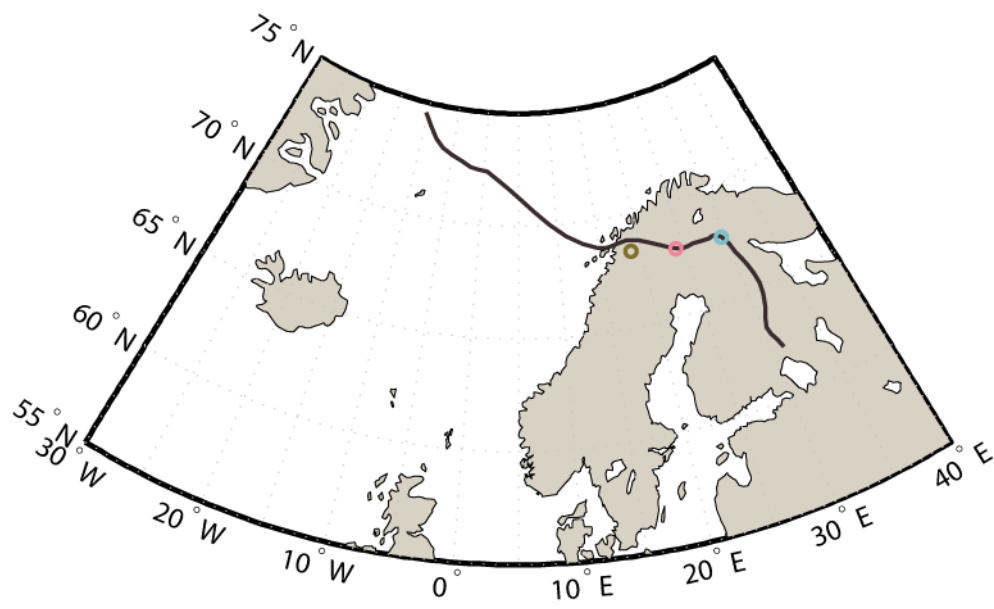
Uncertainty of parameterization

---

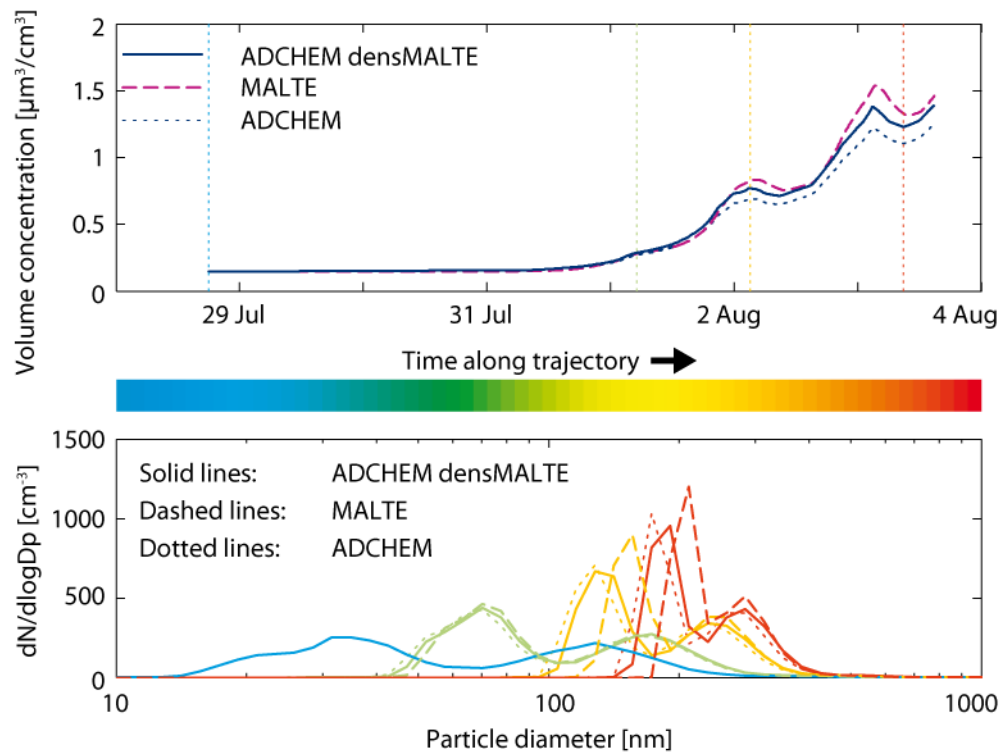
Processes affecting SOA formation	Very uncertain	=>	Less uncertain
First generation volatility- and oxygenation distribution of $\alpha$ -pinene oxidation products	Important		
OH aging rate constant with the gas-phase oxidation products		Important	
Temperature response of the oxidation products		Potentially important	
Fragmentation during aging process (if included)	Important		

4

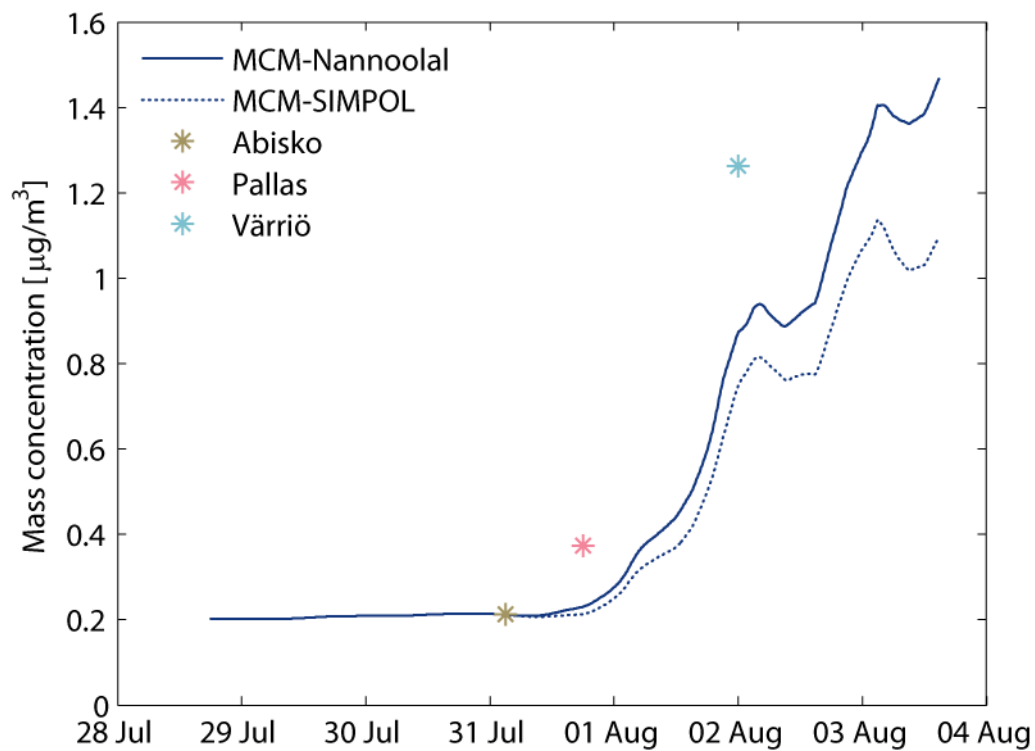
5



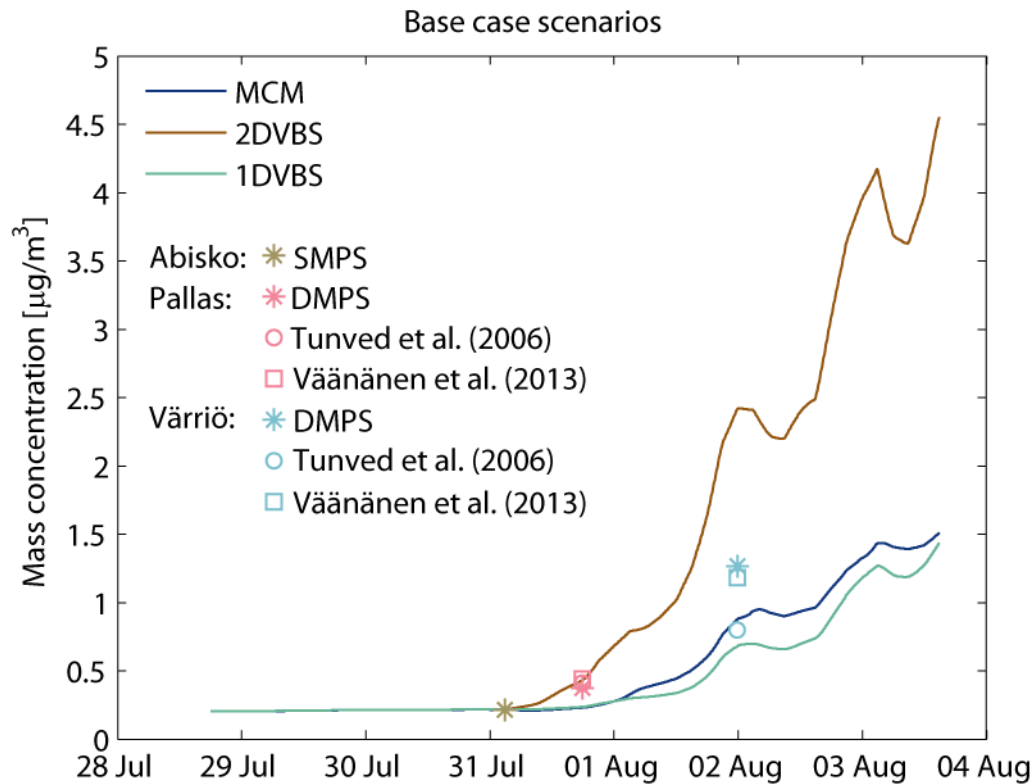
1  
2 Figure 1. The studied air mass trajectory retrieved from the HYSPLIT model. The brown, pink  
3 and blue circles display the location of the measurement stations: Abisko, Pallas and Värriö  
4 respectively.  
5



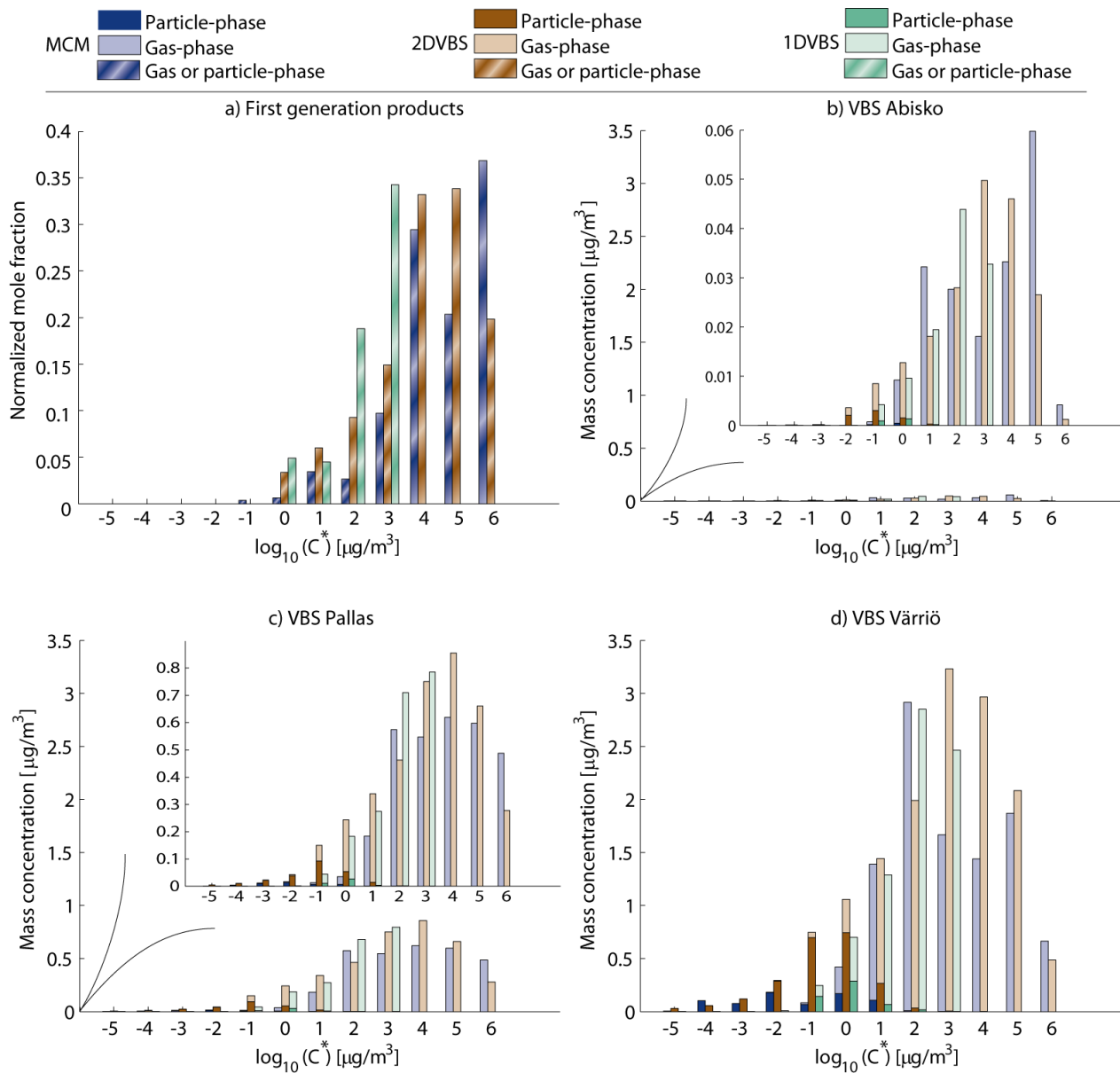
1  
 2 Figure 2. Evolution of particle volume concentration (upper panel) and particle number size  
 3 distribution (lower panel) modeled with the aerosol dynamics box model MALTE-BOX or  
 4 ADCHEM (modeled with a constant SOA density of  $1400 \text{ kg m}^{-3}$  or SOA densities from  
 5 MALTE-BOX). The color of each size distribution plot represents the size distribution at a  
 6 specific time along the trajectory, indicated by the corresponding color of the vertical line in the  
 7 upper panel.  
 8



1  
 2 Figure 3. Particle mass concentration along the air mass trajectory modeled with ADCHEM using  
 3 different methods of estimating the saturation vapor pressures of the organic oxidation products.  
 4

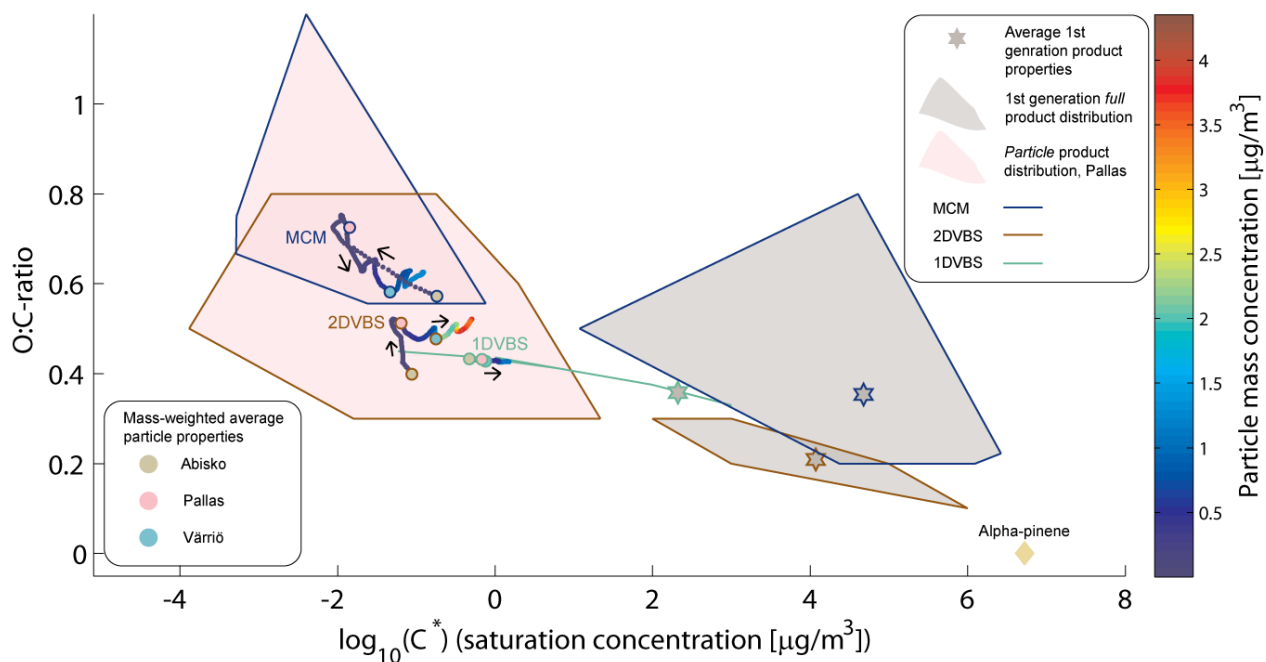


1  
2 Figure 4. Modeled evolution of particle mass along the studied air mass trajectory. The SMPS  
3 (Scanning Mobility Particle Sizer) and DMPS (Differential Mobility Particle Sizer) data points  
4 are the measured size distribution at Abisko, Pallas and Värriö at the time the air mass passed.  
5 Also shown are estimated average mass concentrations as function of time the air mass has spent  
6 over land. The rings are based on measurement during the growing season between 1999-2004  
7 (Tunved et al., 2006) and the squares are based on measurements between 2005-2007 (Väänänen  
8 et al., 2013).  
9

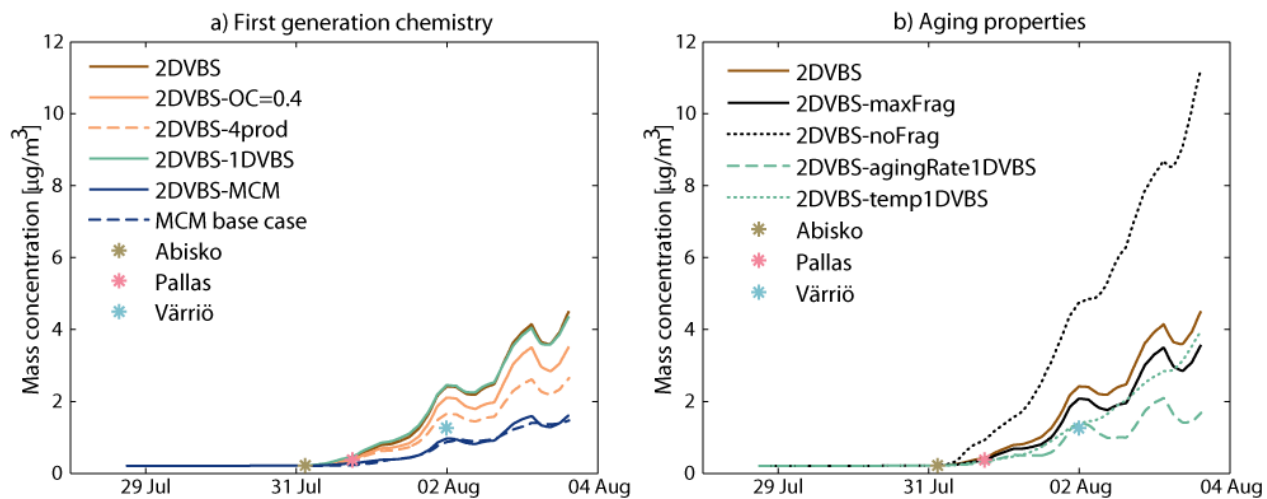


1  
 2 Figure 5. Volatility distribution of the oxidation products in both gas and particle-phase from the  
 3 MCM, 2DVBS and 1DVBS base case simulations. In a) only products from the first oxidation  
 4 step are shown, while b)-d) include products from higher generation oxidation as well. The  
 5 distributions in b)-d) are at Abisko, Pallas and Värriö respectively, the dark colors represent the  
 6 portion of products in the particle phase, and the light colors the portion in the gas phase.

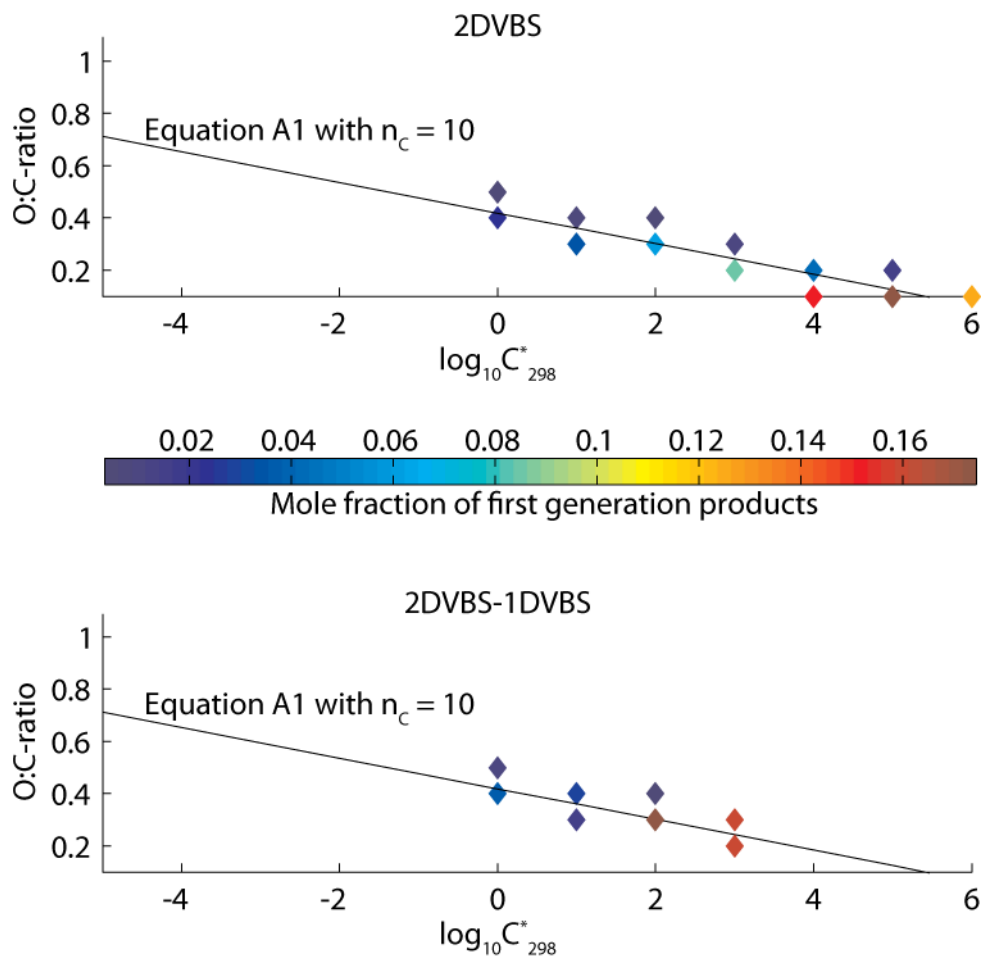
7



1  
 2 Figure 6. The full (gas or particle) first generation distributions of the oxidation products in the  
 3 MCM, 2DVBS and 1DVBS base case simulations are shown as grey areas enclosed with lines  
 4 representing each model simulation (MCM-blue, 2DVBS-brown and 1DVBS-green). The grey  
 5 stars are the corresponding mass-weighted average properties of the first generation products.  
 6 The distributions of the products in particle phase in Pallas are shown as pink areas. Also shown,  
 7 for all three model simulations, are the time evolution (in the direction of the respective arrows)  
 8 of the mass-weighted average particle properties and SOA concentration along the air mass  
 9 trajectory starting from Abisko (beige circles) and passing Pallas (pink circles) and Värriö (blue  
 10 circles).  
 11

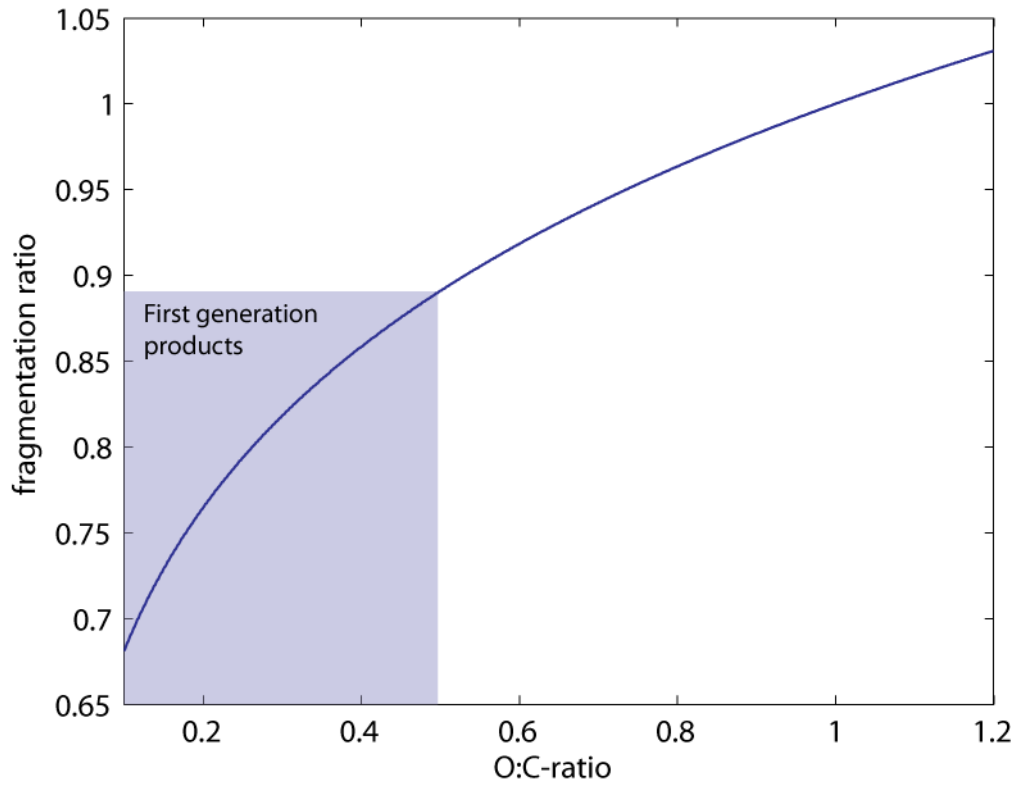


1  
 2 Figure 7. Particle growth along the air mass trajectory modeled with different versions of 2DVBS  
 3 (see Table 3 for more details). In a) different parameterizations of first generation chemistry are  
 4 tested and in b) different parameterizations of gas-phase aging are tested.  
 5



1  
 2 Figure 8. First generation product distribution in the 2-dimensional VBS space modeled with the  
 3 2DVBS simulation (upper panel) and the 2DVBS-1DVBS simulation (lower panel). The black  
 4 line shows the linear dependence between the O:C-ratio and volatility when a carbon number of  
 5 10 is assumed.

6



1  
2 Figure A1. Fraction of products that undergo fragmentation in the 2DVBS-scheme as a function  
3 of their O:C-ratio. The shaded area shows the range of O:C-ratio of the first generation products  
4 in the 2DVBS.